IEEE Access
Multidisciplinary | Rapid Review | Open Access Journal

Received 20 April 2023, accepted 4 May 2023, date of publication 15 May 2023, date of current version 8 September 2023.

Digital Object Identifier 10.1109/ACCESS.2023.3276231

RESEARCH ARTICLE

Development of a Dual-Polarized Direction-Variable Liquid-Crystal Meta-Surface Reflector for Intelligent Reflecting Surface

HIROMI MATSUNO[1], TAKUYA OHTO[1], (Member, IEEE), TAKAHIRO HAYASHI[1], YOSHIAKI AMANO[1], MITSUTAKA OKITA[2], DAIICHI SUZUKI[2], KAZUKI MATSUNAGA[2], AND SHINICHIRO OKA[3]

[1]KDDI Research Inc., Fujimino-shi, Saitama 356-8502, Japan
[2]Japan Display Inc., Nomi-gun, Kawakita-machi 105-0003, Japan
[3]Japan Display Inc., Mobara-shi 297-0037, Japan

Corresponding author: Hiromi Matsuno (hr-matsuno@kddi.com)

ABSTRACT Intelligent reflecting surfaces (IRSs) have been attracting attention as a solution to coverage hole problems in millimeter-wave communication areas. They are considered to be one of the key technologies of next-generation mobile communication systems. Since polarized multiple-input-multiple-output (MIMO) is utilized in millimeter-wave communication systems to deliver high-speed data transmission, an IRS is also required to be applied for polarized MIMO and reflect signals in a wide angle range. To realize an IRS for the polarized MIMO, the IRS is required to reflect the signal of each polarization in the same direction with high isolation. In addition, the IRS is required to control the reflection phase over a wide range. In recent research, many proposals related to the development of IRSs have been proposed. However, since the configuration of a conventional IRS with diodes controls the reflection characteristics by controlling the electric length or shape of the reflecting element, it becomes asymmetrical in the direction of each polarization and it is difficult to apply polarized MIMO. To solve this problem, in this paper, we propose a new design of a dual-polarized liquid-crystal-based IRS for 28 GHz mobile communication systems. Since the proposed IRS controls the reflecting phase by controlling the electric thickness of the substrate, the IRS can control the reflecting phase without changing the shape of the reflecting element. By optimizing the design of the reflecting element, the IRS can achieve a wide reflection phase control of 260 degrees for both vertical and horizontal polarizations. The IRS can also control the reflection direction of each polarization in the range of ± 60 degrees with a high isolation of more than 20 dB. The main contributions of this paper are 1) a proposal for the design of a liquid crystal IRS for polarized MIMO; 2) a proposal of a design method for the liquid-crystal IRS using unit cell analysis; 3) verification of the proposed IRS through electromagnetic field analysis; 4) development of the proposed liquid-crystal IRS; 5) experimental verification of the proposed IRS in an anechoic chamber, and 6) derivation of the MIMO channel capacity of the proposed dual-polarized IRS.

INDEX TERMS Beyond 5G/6G, coverage hole, intelligent reflecting surface, liquid crystal, millimeter wave, polarized MIMO, channel capacity.

I. INTRODUCTION

A. BACKGROUND

In fifth-generation mobile communication systems (5G), millimeter-wave bands with wide bandwidths are utilized to deliver high data rates and low-latency mobile communication services [1]. These high-frequency bands are also expected to be utilized in beyond 5G/6G mobile networks to satisfy the increasing demand for communication quality. On the other hand, these frequency bands suffer from high blockage loss due to their rectilinear propagation characteristics. This creates coverage holes where a signal

The associate editor coordinating the review of this manuscript and approving it for publication was Barbara Masini.

from a base station (BS) is insufficient to provide high communication quality in the communication area [2].

To overcome the coverage holes, deploying a passive reflector is an attractive method to enhance the received power in the coverage holes economically and ecologically compared to installing additional BSs and wireless repeaters. In particular, in utilizing meta-surface reflectors, which have an artificial surface to reflect signals in the designed direction, the capability of the reflector is enhanced by reducing the deployment restriction of the conventional reflectors [3]. In addition, since the coverage holes change due to the appearance and disappearance of physical obstacles such as new buildings and growing trees [4], an intelligent reflecting surface (IRS) that can control the reflection direction, has been gathering attention. Since IRSs can enhance various aspects of communication quality such as coverage, channel capacity, diversity gain, etc., IRSs are considered to be one of the key technologies for next-generation mobile communication systems [5], [6], [7], [8], [9], [10], [13].

Since coverage holes are caused in a wide area of the BS, an IRS is required to reflect signals from the BS in the desired direction over a wide range. In addition, the polarized multiple-input-multiple-output (MIMO) is utilized in millimeter-wave mobile communication systems to deliver high-speed data transmission [11]. Therefore, by applying an IRS for polarized MIMO, both the coverage and data-transmission speed are enhanced in the target area of the IRS [12].

B. RELATED WORKS

IRSs are designed to arrange the reflection phase in unit cells that are periodically placed at sub-wavelength intervals on the reflecting surface. The reflection direction is controlled by controlling the reflection phase of each unit cell. Since the reflection phase distribution on the reflecting surface determines the reflection direction, the reflection phase of each unit cell is required to be controlled with a wide reflection range and high resolution [13].

The channel capacity of polarized MIMO is maximized when the received signal of each polarization is isolated with the same signal strength [14]. To achieve high isolation between each polarization, the reflection power of the cross-polarized component should be suppressed. Therefore, IRS should be designed using cross-polarization discrimination (XPD) as a design parameter. To achieve the same signal strength, since the reflection pattern, which is the angular characteristic of the reflection power, depends on the reflection phase and amplitude of each unit cell, the unit cell should be designed to achieve the same reflection phase and amplitude for each polarization.

The authors of [15] analytically investigated the relationship between the MIMO capacity and XPD of the IRS. Assuming a non-line-of-sight (NLOS) environment between the BS and the user equipment (UE) and a line-of-sight (LOS) environment between each BS and IRS and UE and IRS, an XPD of more than 10 dB is required to provide the strong effects of polarized MIMO. Regarding the signal strength of each polarization, assuming the aforementioned environment, the direction of each BS and UE from the IRS does not change owing to the polarization. Therefore, reflection characteristics such as reflection direction and reflection power are required to be designed equally for each polarization to provide the equivalent signal strength of each polarization.

The development of an IRS requires improvement of the reflection phase control functions [16]. Recently, many types of IRS using P-intrinsic-N (PIN) diodes and varactor diodes have been reported [17], [18].

The authors of [17] developed an IRS with three layers comprising a patch plane, slot-loaded plane, and ground plane. The slot-loaded plane has four slot configurations, and by switching them with the placement of five PIN diodes, four reflection directions, i.e., 0, 20, 40, and 60 degrees are achieved. However, since the IRS can only control four reflection conditions, it is insufficient to reflect signals in the desired directions over a wide range. In addition, since the diode-based IRS controls the reflection phase by controlling the electric length of the reflecting element, the reflecting characteristics depend on the direction of current flow on the reflecting element. This causes differences in the reflection characteristics of each polarization.

To solve these problems, the authors of [18] developed a dual-polarized IRS with varactor diodes, which alternately arranges reflecting elements for each vertical and horizontal polarization. By applying the varactor diodes to the reflecting element, the reflection phase is continuously controlled by the bias voltage. In addition, by arranging the reflecting element for each polarization, the IRS can independently control the reflection phase for each vertical and horizontal polarization. However, due to deployment restrictions, the IRS has an asymmetric configuration. This causes differences in the reflection characteristics of each polarization. The reflection phase control range for the horizontal polarization is 150 degrees although that for the vertical polarization is 250 degrees. In addition, the isolation between each polarization changes as the bias voltage of each polarization changes. This indicates that the IRS cannot reflect the signals of each polarization in the desired direction with high isolation.

As another reflection phase control function, recent research on new materials has been gathering attention. The authors of [19] focus on liquid-crystals (LCs) to control the reflection phase. By controlling the bias voltage of the LC, the IRS continuously controls a reflection phase of more than 270 degrees at 47 GHz. However, the reflecting elements of the IRS are designed as dipole elements to achieve a wide reflection phase range. Therefore, the IRS has an asymmetrical configuration in the direction of each orthogonal polarization and cannot be applied to polarized MIMO.

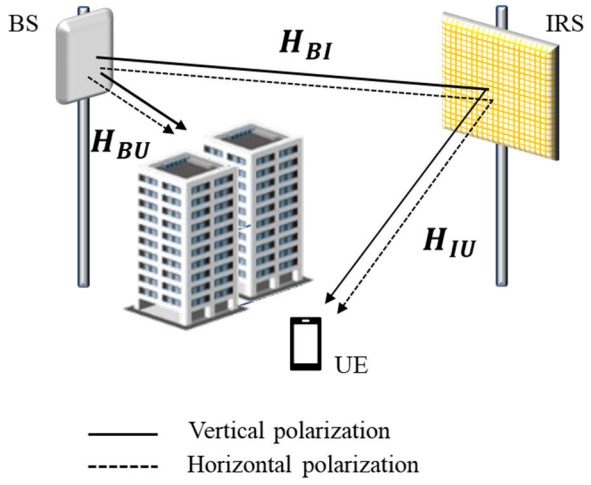

FIGURE 1. The System model of IRS for polarized MIMO. In this case, each vertical and horizontal polarization is considered.

As mentioned above, there have been many reports of IRS development. However, since it is difficult to reflect each polarized signal in the same reflection characteristics within high isolation, the development of a polarized MIMO IRS is challenging.

C. CONTRIBUTION

To address these problems, we proposed an LC IRS for 28 GHz mobile communication systems [20], [21]. The proposed LC IRS was designed with the configuration of an electrode, LC, and ground layers. The dielectric permittivity of the LC is controlled by the bias voltage between the electrode and ground. In contrast to a diode-based IRS, the reflection phase is controlled by the electric thickness of the reflecting element. Since the configuration of the reflecting element does not change, the IRS is expected to achieve the same reflection characteristics for each polarization. In this paper, to achieve a wide reflection phase and high isolation between each polarization, the configuration of each electrode and the bias line was optimized.

Through an evaluation using an electromagnetic (EM) simulator [22] and measurements, the proposed IRS can control each vertical and horizontal polarization in the range of 260 degrees. In addition, the IRS can control reflection direction within ±60 degrees with a high XPD of more than 20 dB.

The main contributions of the proposed paper are summarized as follows:

1) Proposal of an LC IRS design for polarization MIMO, which controls a reflection direction of ±60 degrees with a high XPD of more than 20dB;
2) Proposal of the design method of LC IRC using an equivalent circuit model;
3) Verification of a proposed LC for an IRS through EM field analysis;
4) Development of the proposed LC IRS;
5) Verification of the proposed LC IRS through measurements in an anechoic chamber; and
6) Derivation of the MIMO channel capacity for the polarized MIMO.

D. ORGANIZATION

The remainder of this paper is organized as follows. The system model of the polarized MIMO and the design of the LC IRS for polarized MIMO are introduced in Section II. In Section III, the unit cell of the LC IRS was analyzed using an equivalent circuit model and an EM simulator. In Section IV, the LC IRS with 24×24 elements was analyzed using an EM simulator. In Section V, the measurement results of the developed LC IRS were evaluated. This paper is concluded in Section VI.

II. SYSTEM MODEL AND DESIGN TARGETS OF DUAL-POLARIZED IRS

A. SYSTEM MODEL

The system model of the IRS for polarized MIMO is shown in Fig. 1. For simplicity, we consider a single-user MIMO model. The BS transmits signals with each vertical and horizontal polarization antenna. Each signal is reflected at the IRS and received by the UE. The received signal of the UE is expressed as

$$\mathbf{y} = \mathbf{H}\mathbf{x} + \mathbf{n} \tag{1}$$

Here, $\mathbf{x}$and$\mathbf{n}$denote the transmitting signal and the noise vectors, respectively. $\mathbf{H}$denotes the channel matrix of $K \times K$ MIMO. The channel capacity is calculated as follows:

$$\mathbf{C} = \Sigma_{k=1}^{K} (\lambda_k \gamma + 1) \tag{2}$$

where, γ and $\sqrt{\lambda_k}$ denote the signal-to-noise ratio (SNR) and the k-th eigenvalue of the channel matrix, respectively. The channel capacity is maximized when the channel matrix $\mathbf{H}$ becomes full rank; therefore, the non-orthogonal components of $\mathbf{H}$should be minimized to achieve an increased MIMO channel capacity.

Assuming polarized MIMO and that only the signal from the IRS is observed at the UE ($\mathbf{H}_{BU} \cong \mathbf{O}$), the channel matrix $\mathbf{H}$is expressed by multiplying the gain of BS, $\mathbf{G_{BS}}$, the channel matrix between each BS and IRS, $\mathbf{H_{BI}}$, the reflecting gain of the IRS, $\mathbf{G_{IRS}}$, the channel matrix between each IRS and UE, $\mathbf{H_{BI}}$, and the gain of UE, $\mathbf{G_{UE}}$ as follows [15]:

$$\mathbf{H} = \mathbf{G_{BS}}\mathbf{H_{BI}}\mathbf{G_{IRS}}\mathbf{H_{IU}}\mathbf{G_{UE}}. \tag{3}$$

Here, $\mathbf{H_{BI}}$, $\mathbf{H_{IU}}$, $\mathbf{G_{BS}}$, $\mathbf{G_{UE}}$, and $\mathbf{G_{IRS}}$aredivided into vertical polarization components, $|\cdot|_V$, horizontal polarization components, $|\cdot|_H$, and cross-polarized components, $|\cdot|_X$ as

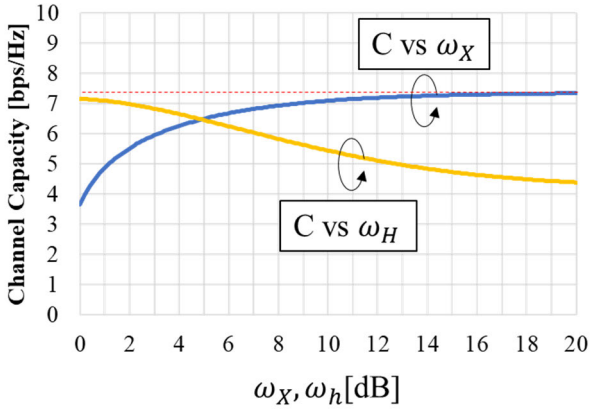

FIGURE 2. Channel capacity by changing the cross-polarization discrimination and gain difference of IRS. Design of the unit cell of a conventional IRS.

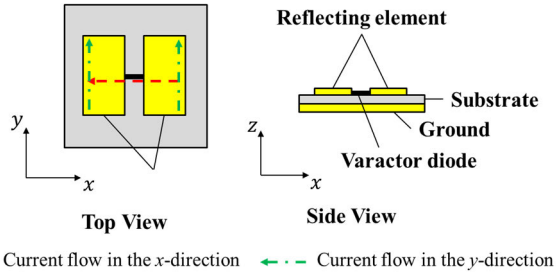

FIGURE 3. Unit cell configuration of a conventional IRS [16].

follows:

$$\mathbf{H_{BI}} = \begin{bmatrix} h_{BI,V} & h_{BI,X} \\ h_{BI,X} & h_{BI,H} \end{bmatrix}, \mathbf{H_{IU}} = \begin{bmatrix} h_{IU,V} & h_{IU,X} \\ h_{IU,X} & h_{IU,H} \end{bmatrix}, \tag{4}$$

$$\mathbf{G_{BS}} = \begin{bmatrix} g_{BS,V} & g_{BS,X} \\ g_{BS,X} & g_{BS,H} \end{bmatrix}, \mathbf{G_{UE}} = \begin{bmatrix} g_{UE,V} & g_{UE,X} \\ g_{UE,X} & g_{UE,H} \end{bmatrix}, \tag{5}$$

$$\mathbf{G_{IRS}} = \begin{bmatrix} g_{IRS,V} & g_{IRS,X} \\ g_{IRS,X} & g_{IRS,H} \end{bmatrix} \tag{6}$$

B. TARGETS OF THE IRS FOR POLARIZED MIMO

To clarify the requirements of the dual-polarized IRS, the channel capacity in the coverage hole is evaluated by changing the cross-polarization discrimination (XPD) and the gain difference of the IRS. The XPD of IRS is defined as $\omega_X = g_{IRS,V}/g_{IRS,X}$. The difference in the reflection gain of the IRS is also defined as $\omega_H = g_{IRS,V}/g_{IRS,H}$. Regarding the XPD of each BS and UE, approximately 20 dB and 6 dB are expected, respectively [23], [24]. In addition, the expected XPR of the urban micro street canyon model is 9 dB on average [25]. Channel capacity is evaluated using (3) and the expected values above.

Figure 2 shows the channel capacity of the polarized MIMO when the SNR = 20 dB. By increasing ω_X, channel capacity increases. It also converges to about 7 bps/Hz around $\omega_X \cong$ 15dB, and therefore, the target XPD of the IRS might be 15 dB. However, the channel capacity decreases with increasing ω_H. Since the inflection point is approximately 4 dB, the channel capacity degrades rapidly when ω_H is greater than 4 dB. From these results, the proposed IRS is designed to satisfy ω_X of over 15 dB and ω_H of less than 4 dB.

TABLE 1. Electrical constants of LC [26].

Symbol	Quantity	Value
$\varepsilon_{\parallel}$	Permittivity	2.98
$\varepsilon_{\perp}$	Permittivity	2.53
$\tan\delta_{\parallel}$	Loss tangent	0.009
$\tan\delta_{\perp}$	Loss tangent	0.022

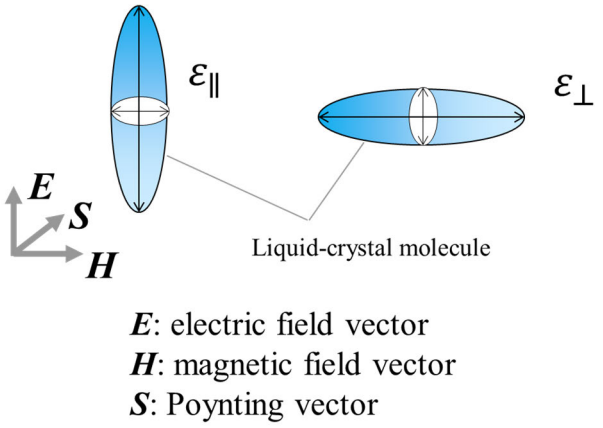

FIGURE 4. Configuration of the LC molecule and its electrical features.

III. DESIGN OF THE PROPOSED IRS

A. CONVENTIONAL DESIGN OF AN IRS

An IRS is designed using meta-surface techniques. It is designed to arrange the reflection phase in unit cells that are periodically placed at sub-wavelength intervals on the reflecting surface. Once the incident wave impinges on the IRS, current is induced in the unit cell. Since the current also radiates the reflection wave, the reflection phase is controlled by the phase-shift function designed in the unit cell.

Figure 3 shows the unit cell configuration of a conventional IRS [15]. A unit cell consists of a reflecting element, a substrate, and a ground plane. The reflecting element also consisted of two patch elements connected to a varactor diode. The reflection phase can be controlled by controlling the capacitance of the varactor diode.

However, the current flow on the reflecting element has directivity that depends on the polarization of the incident wave. When the incident wave is polarized in the x-direction, current flows in the x-direction. Since the diode is connected in the x-direction, the current flows in the diode, and the reflection phase are controlled. However, since the current in the y-direction does not flow in the diode, the reflection phase of the incident wave polarized in the y-direction cannot be controlled using this configuration. This asymmetry creates a reflection phase difference between each polarization.

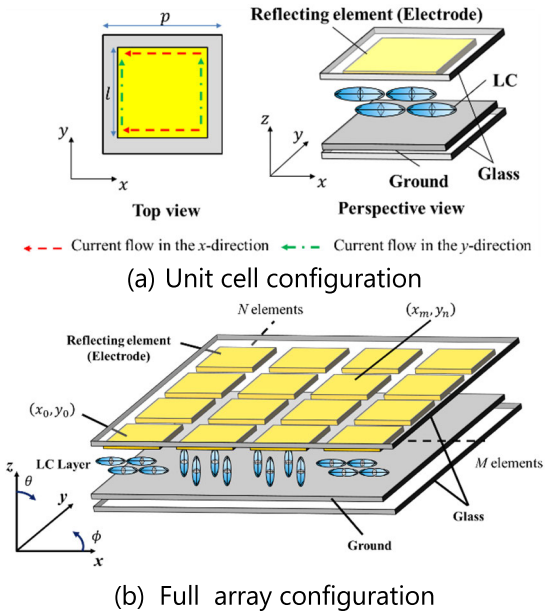

FIGURE 5. Unit cell and full array configuration of the proposed IRS.

The authors of [18] also proposed arranging an adjacent unit cell with a rotation angle of 90 degrees to reflect each orthogonal polarization. However, the reflection phase of each polarization differs by more than 100 degrees owing to the implementation limitations. This indicates that a conventional IRS cannot control the reflection direction of each polarized signal in the same direction.

B. DESIGN OF THE PROPOSED LC IRS

To solve these problems, we proposed an LC meta-surface reflector for IRS [20]. In contrast to a conventional IRS, the reflection phase control function is deployed in the substrate between the reflecting element and ground plane. Owing to its configuration, the LC IRS is designed to remain in a rotationally symmetric configuration, which achieves reflection control of each orthogonal polarization. In this paper, an LC IRS for polarized MIMO was designed.

1) FEATURES OF THE LC

Figure 4 shows the configuration of the LC molecules. LC are molecules with dielectric anisotropy. The electromagnetic characteristics of an LC depend on the relationship between the electric field vector **E** and the orientation of the LC molecule. Each dielectric permittivity and loss tangent of the long axis and short axis of the LC molecule is defined as $\varepsilon_{\parallel}$ and $\tan\delta_{\parallel}$, and $\varepsilon_{\perp}$ and $\tan\delta_{\perp}$, respectively. Referring to [26], the electrical constants of the LC are listed in Table 1. Since the direction of the LC molecules is controlled by the bias voltage applied to the LC, the electromagnetic constants of the LC are electrically controlled. Using this feature, the LC is utilized as a phase shifter, and reflection phase control is expected [27], [28].

The phase shift of the LC depends on the thickness of the LC. Considering the thickness of the LC t and the wavelength

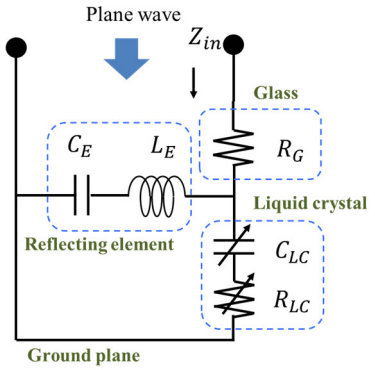

FIGURE 6. Equivalent circuit of the LC IRS assuming the plane wave impinging in the IRS.

λ, the phase shift of the LC $\Delta\sigma$ is calculated as the difference in the path length:

$$\Delta\sigma = 2\pi t/\lambda\left(\sqrt{\varepsilon}_{\parallel} - \sqrt{\varepsilon}_{\perp}\right) \tag{7}$$

Since the difference in permittivity is small, the thickness t requires several wavelengths to achieve a sufficient phase shift to control the reflection direction. However, owing to manufacturing restrictions, it is difficult to increase the thickness of the LC layer.

2) PROPOSED LC IRS

To enhance the reflection phase shift, in this paper, both the resonance of the reflecting element and permittivity control of the LC are utilized. Figure 5 shows the unit cell configuration of the proposed LC IRS. The LC layer is inserted between the ground plane and the electrode. The permittivity of the LC is controlled by the bias voltage between the ground plane and the electrode. To maintain the LC layer in the structure, the glass substrates are placed above the electrode and below the ground plane. Here, the electrode was also utilized as a reflecting element, which determines the reflecting characteristics.

The reflecting element must be designed to be rotationally asymmetric in both the x- and y-direction to achieve the same reflection characteristics for both x- and y-polarization. In addition, when the current flow includes a non-orthogonal component, the current generates cross-polarization in the reflecting wave. Therefore, a reflecting element is required to maintain orthogonality in each polarization direction. Therefore, in this paper, a rectangular patch was applied for the reflecting element.

IV. DESIGN AND ANALYSIS

1) EQUIVALENT CIRCUITS OF THE LC IRS

To symmetrically design the LC IRS, we applied an equivalent circuit model. Considering that the plane wave impinges on the IRS, which consists of reflecting an element and a ground plane, a current is induced on the reflector.

Some of the current flows on the reflecting element, and the rest flows on the ground plane. Therefore, the equivalent circuit of the LC IRS is expressed as a parallel circuit of the

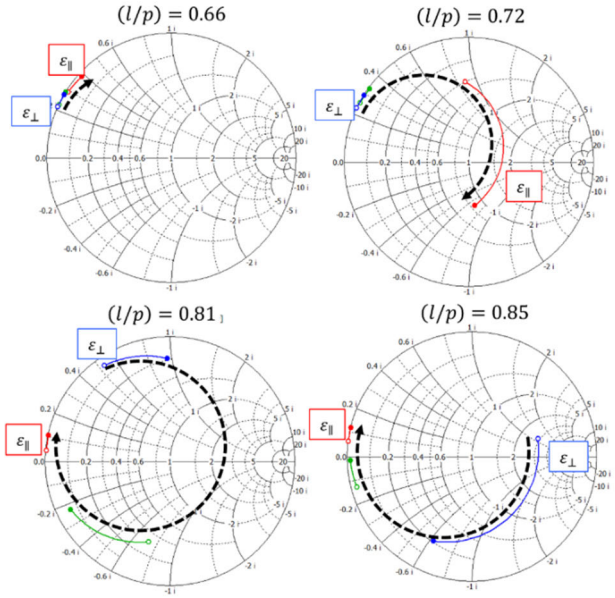

FIGURE 7. Reflection impedance by changing (l/p).

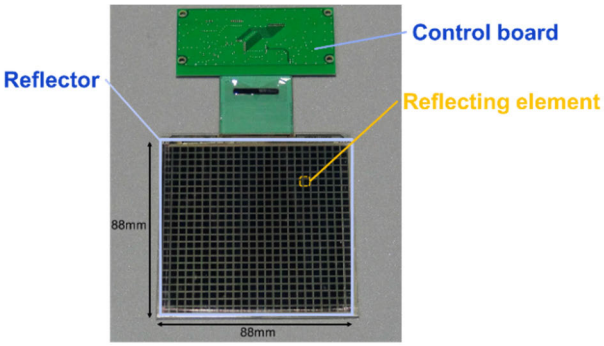

FIGURE 8. Prototype of LC IRS for 28 GHz. The IRS consists of 24 × 24 reflecting elements.

reflecting element and ground plane as shown in Fig. 6. The current flow on the ground plane passes the LC layer. The permittivity and the loss tangent of the LC are controlled by bias voltage, and it is expressed as the variable capacitance and resistance, C_{LC} and R_{LC}, respectively.

From the equivalent circuit, the input impedance Z_{in} of the unit cell is expressed by the following equation:

$$Z_{in} = A + jB \tag{8}$$

$$A = R_G + R_{LC}\left(\omega L_E - \frac{1}{\omega C_E}\right)^2 \tag{9}$$

$$B = \left(\omega L_E - \frac{1}{\omega C_E}\right) \times \left(R_{LC}^2 - \frac{L_E}{C_{LC}} + \frac{1}{\omega^2 C_{LC}}\left(\frac{1}{C_E} + \frac{1}{C_{LC}}\right)\right) \tag{10}$$

Here, j is a unit imaginary number and $\omega = 2\pi f$ is the angular frequency. For a rectangular patch element, the inductance and capacitance of the reflecting elements, L_E and C_E, are

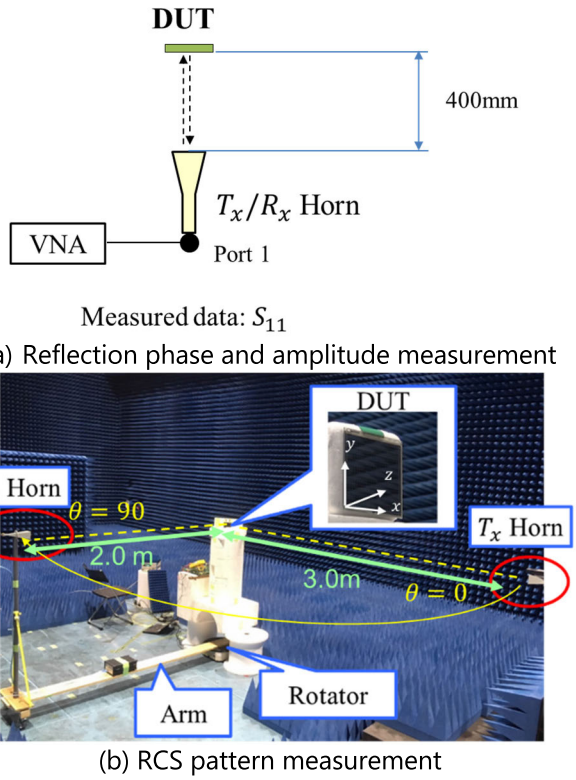

FIGURE 9. Measurement setup.

expressed as follows [28]:

$$\omega L_E = \frac{p}{\lambda}\left[\ln\csc\left(\frac{\pi l}{2p}\right) + G(p, l, \lambda)\right]\left(\frac{l}{p}\right) \tag{11}$$

$$\omega C_E = \frac{4p}{\lambda}\left[\ln\csc\left(\frac{\pi l}{2p}\right) + G(p, l, \lambda)\right]\left(\frac{l}{p}\right) \tag{12}$$

where p, l, and $G(p, l, \lambda)$ denote the length of the unit cell, length of the patch element, and gain of the patch element, respectively. From (11) and (12), the reflection impedance, Z_{in}, depends mainly on (l/p). Therefore, the IRS is designed by changing (l/p).

2) PARAMETER STUDY

In the previous section, the input impedance of the proposed LC meta-surface reflector also depended on (l/p). In this section, we evaluated the input impedance using a commercial FDTD simulator [21] by changing (l/p). To avoid sidelobe, the size of the unit cell p was set to less than 0.5λ.

Figure 7 shows the reflection impedance obtained by changing l/p. The figure shows the simulation results for a frequency range of 27.8 – 28.2 GHz. The blue, green, and red lines show the reflection impedances of the lowest, middle, and highest permittivies, respectively. Since the permittivity of the LC varies continuously, the locus from the blue line to the red line, which is the black dashed arrow in the figure, is the reflection impedance shift caused by changing the permittivity of the LC. The inner angle of the black dashed arrow indicates the phase shift and the distance from the center (normalized impedance) to the locus indicates

the reflection amplitude of the LC. When the amplitude was lowered, the reflection loss increased. Therefore, the parameters should be optimized to achieve a large inner angle, which indicates the phase shift, and avoid close-to-normalized impedance. In the simulation results, the radius of the locus increased as l/p increased. This implies that the reflection loss is reduced with a large l/p. However, when l/p is 0.8 l, the inner angle of the locus is the largest among the four. To achieve both high reflection phase control and low reflection loss, we optimized the parameters to achieve the lowest loss satisfying a phase shift of more than 270 degrees.

3) PROTOTYPE

Based on the analysis in Fig. 7, the LC meta-surface reflector was developed for the 28 GHz band. An overview of the prototype is presented in Fig. 8. The size of the prototype was 88 mm $\times$88 mm and the number of reflecting elements was 24 $\times$24. The bias voltage was controlled by the control PC via a control board.

Regarding the configuration of the bias voltage, the prototype has 256 states of bias voltage, and the reflection phase is therefore continuously controlled compared with that of PIN diodes.

V. SIMULATION AND MEASUREMENT

1) SIMULATION METHOD

The simulation was performed using the commercial FDTD method [19]. The reflection phase and reflection amplitude were calculated through unit cell analysis using the Floquet periodic boundary conditions. In the unit cell analysis, the plane wave impinged from the front of the unit cell and the reflection impedance, S_{11}, was calculated. The radar cross-section (RCS) pattern of the meta-surface reflector was evaluated through a full model analysis using perfectly matched layer boundary conditions. The plane wave impinged from the front of the meta-surface reflector and the far-field RCS pattern was calculated.

2) MEASUREMENT METHOD

The measurement was performed in an anechoic chamber. Figure 9 shows the measurement setup. The reflection phase and amplitude were obtained by measuring S_{11} of the reflector using a vector network analyzer (VNA). The plane wave impinges from the transmitting (Tx) horn antenna, which is defined as port 1, in front of the device under test (DUT). The reflected signal was received using the same horn antenna.

In the measurement, the distance from the Tx antenna and DUT were set at 400 mm. Since the meta-surface reflector was implemented with 24 $\times$ 24unit cells, the reflection phase and amplitude of each unit cell were difficult to measure directly. Therefore, the reflection phase and amplitude of the entire 24 $\times$ 24 unit cells were measured by setting the same bias voltage to each unit cell. In addition, since the measured S_{11} includes propagation characteristics between the meta-surface reflector and the horn antenna, the reflection phase and amplitude of the meta-surface reflector are evaluated by calculating the difference of each S_{11} of the DUT and reflector whose reflection characteristics are known. Since the reflection amplitude and phase of the metal plate are 0 dB and 180 degrees, we utilized a metal plate for calibration. The measured S_{11} of the DUT and the metal plate are defined as $S_{11,DUT}$ and $S_{11,Metal}$, respectively. The reflection phase and amplitude of the DUT, φ and A, were calculated using the following equations:

$$\varphi = \arg\left(S_{11,DUT} - S_{11,Metal}\right) \tag{13}$$

$$A = \left|S_{11,DUT} - S_{11,Metal}\right| \tag{14}$$

Regarding the RCS pattern, the plane wave impinges on the DUT from the Tx horn antenna in front of the DUT and receives the signal with the receiving (Rx) horn antenna, which is defined as port 2, at angle θ_r. In the measurement, the distance between the DUT and each Tx and Rx horn antenna is set at 3.0 m and 2.0 m, respectively to satisfy the far field conditions. S_{21} was measured by changing θ_r from 0 to 90 degrees to obtain the RCS pattern. To evaluate the cross-polarization discrimination of the IRS, the polarization of each transmitting and receiving horn antenna was rotated while maintaining the IRS setting. Since the polarization direction was parallel and orthogonal to the x and y-direction, we evaluated each x- and y-polarized incident wave. The co-polarization (CP) of the x-polarization indicates the received power of the x-polarized incident wave with the x-polarized horn antenna. Cross-polarization (XP) of the x- polarization is the received power of the y-polarized incident wave with the x-polarized horn antenna.

3) EVALUATION OF THE REFLECTION PHASE AND AMPLITUDE

Figure 10 (a) shows the simulated and measured reflection phases and amplitudes for the x-polarization at 28 GHz. The plot shows the observation point for the same bias voltage. In the figure, each simulated and measured reflection phase was changed from 0 to -270 degrees by changing the bias voltage. In addition, each simulated and measured reflection amplitude was changed between 0 to -7 dB. Figure 10 (b) shows the reflection phase and amplitude for y-polarization. Similar to that of x-polarization, each simulated and measured reflection phase was changed from 0 to -270 degrees and each reflection amplitude was changed between 0 and -7 dB by changing the bias voltage. These results verified the validity of the proposed IRS design method.

Figure 10 (c) shows a comparison of the reflection phase and amplitude for each polarization. Each polarization had a similar curve. This implies that the proposed IRS can control the reflection direction of each orthogonal polarization in the same direction. The maximum difference between each

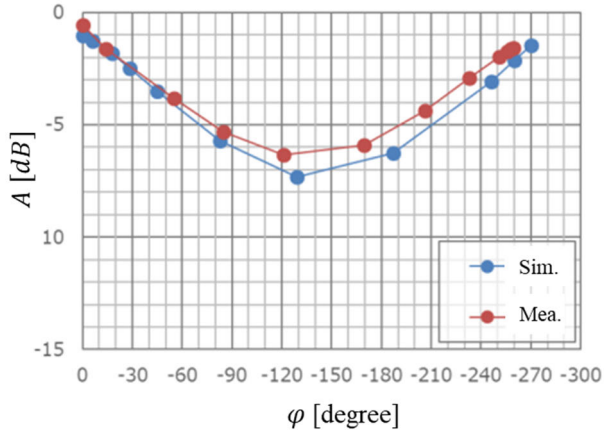

(a) x-polarization

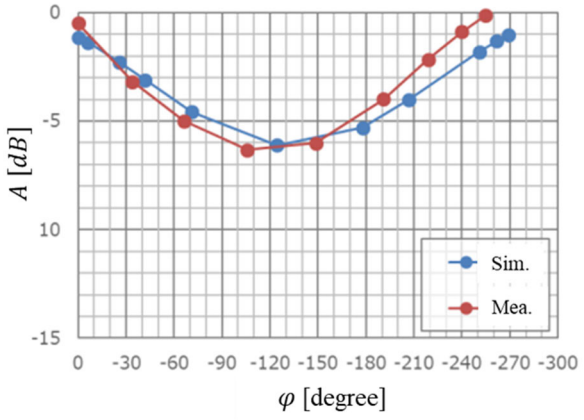

(b) y-polarization

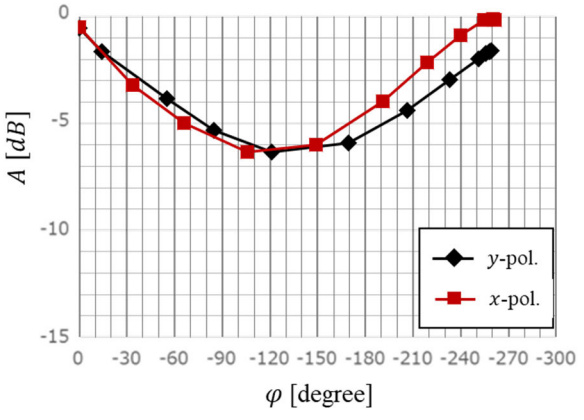

(c) Comparison of polarization

FIGURE 10. Reflection phase and amplitude.

reflection phase and amplitude of the same bias voltage is 27 degrees and 1.5 dB, respectively.

4) EVALUATION OF THE RCS PATTERN

To evaluate the angular characteristics of the LC IRS, the RCS patterns are designed with the measured reflection phase. Considering the incident angle (θ_i, ϕ_i) and reflection angle (θ_o, ϕ_o), the reflection phase of the unit cell at the location (x_m, y_n), σ_{mn}, is calculated using the following equation.

$$\sigma_{mn} = \frac{2\pi}{\lambda}\{x_m(\sin\theta_o\cos\phi_o - \sin\theta_i\cos\phi_i) + y_n(\sin\theta_o\sin\phi_o - \sin\theta_o\sin\phi_o)\} \quad (15)$$

In this paper, the RCS patterns were designed to reflect the incident wave from the front of reflector ($\theta_i = 0$) to the zx-plane.

Figure 11 shows the RCS pattern of the proposed LC IRS. The reflection phase of each unit cell was designed to reflect the incident wave at a reflection angle of $(\theta_o, \phi_o) = (-15, 0)$, $(-30, 0)$, $(-45, 0)$, and $(-60, 0)$, respectively. The black solid line in the figure shows the reflection pattern of x-polarization of the x-polarized incident wave (X_{CP} is defined as the co-polarized reflection pattern of x-polarization). The black dashed line shows the reflection pattern of y-polarization of the x-polarized incident wave (X_{XP} is defined as the cross-polarized reflection pattern of x-polarization). Similarly, the red solid line and dashed line show the co-polarized and cross-polarized reflection patterns of the y-polarized incident wave, Y_{CP} and Y_{XP}, respectively. As shown in the figure, each reflection pattern is directed to the desired reflection angle, and the proposed LC IRS can therefore control the reflection angle over a wide range.

Regarding the difference in reflection power between each polarization, ω_H, each reflection pattern in Fig. 11 has a small difference of less than 1.6 dB. Regarding the cross-polarized reflection, ω_X,each reflection pattern in Fig. 11 exhibits a low cross-polarized reflection. XPD of approximately 20 dB was achieved, as summarized in Table 2.

TABLE 2. Reflection Ability of Proposed LC IRS.

	Reflection angle	(ω_H, ω_X)
Conventional [18]	$(45, 0)$	$(2.89, -)$
Proposed	$(15, 0)$	$(0.49, 20.3)$
	$(30, 0)$	$(1.22, 19.9)$
	$(45, 0)$	$(1.6, 22.4)$
	$(60, 0)$	$(0.52, 22.0)$

5) MIMO CAPACITY EVALUATION

As discussed in Section II, the channel capacity of polarization MIMO depends on the reflection power difference ω_H and cross-polarization discrimination, ω_X of the IRS. To evaluate the channel matrix of the proposed LC IRS, we compared it with the conventional dual-polarized IRS in [18].

The reflection phase of the IRS was controlled from 0 to 260 degrees for one polarization, and from 0 to 180 degrees for another polarization. This creates a difference in the reflected power. Figure 12 shows the reflection pattern design using the reflection phase in [18] with the same reflecting element configuration as that in Fig.11. Due to the restriction of the reflection phase control range, there are

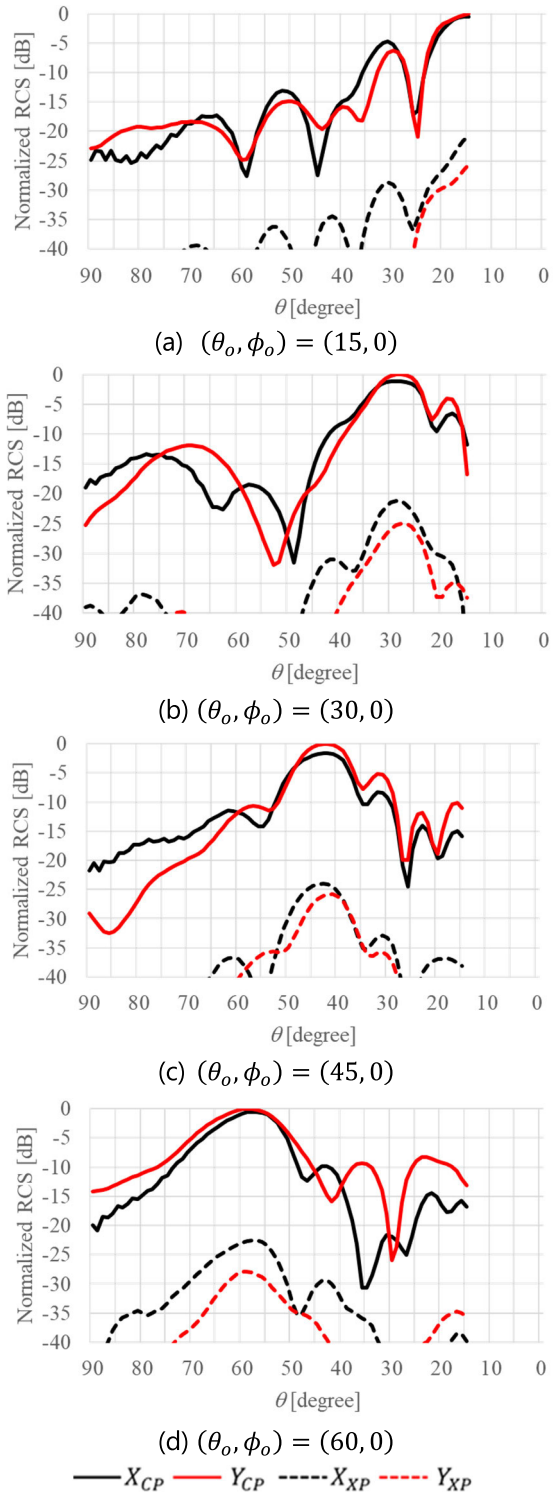

FIGURE 11. Measured RCS Pattern.

differences in the reflection power for each x-polarization and y-polarization. The differences in the reflection power, ω_H, of $(\theta_o, \phi_o) = (45, 0)$ are 2.89 dB.

Regarding the isolation between each polarization, the IRS in [18] can control the isolation of each unit cell in the range of 0 to 16 dB by changing the bias voltage of the varactor diode. Therefore, we assume the isolation of the conventional IRS to be 16 dB in the best case. On the other hand, since various values of bias voltage are applied to design the reflection pattern, we assume the isolation of the conventional IRS 5.5 dB, which is the average value of the true value.

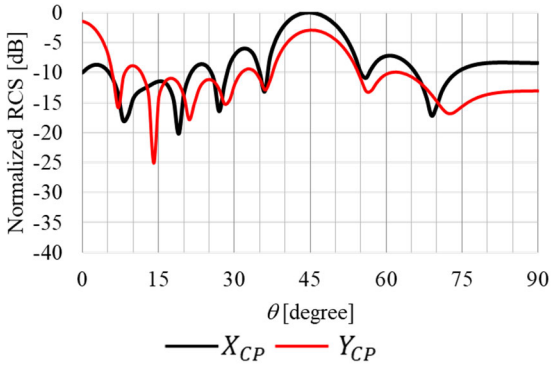

FIGURE 12. Calculated RCS pattern using reflection phase in [18].

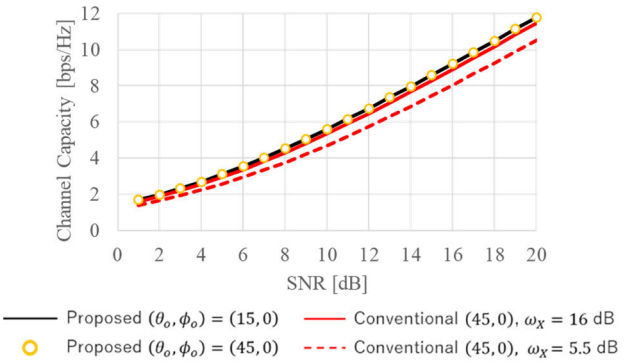

FIGURE 13. Channel capacity of proposed LC IRS and conventional IRS in [18].

Figure 13 shows the channel capacities of the proposed LC IRS and the conventional IRS. The isolation of the conventional IRS was set at 16 dB for the best case and 5.5 dB for the average case. From the figure, since the proposed LC IRS achieves a low reflection power difference and high isolation between each polarization, the channel capacity of the proposed LC IRS is higher than that of the conventional IRS, especially compared with that of ω_X = 5.5dB. In addition, since ω_H and ω_X of the proposed IRS do not depend on the reflection direction, the proposed IRS can reflect signals with highly polarized MIMO channel capacities.

VI. CONCLUSION

In this paper, a novel LC IRS for polarized MIMO is proposed and developed. Since polarized MIMO is utilized in mobile communication systems, an IRS is also required to be applied for polarized MIMO to enhance both coverage and channel capacity. To achieve an IRS for polarized MIMO, the reflection signal strength of each orthogonal polarization is required to be the same with high isolation.

Since the conventional diode-based IRS controls the reflection characteristics by changing the electric length of the reflecting element, it has an asymmetric configuration in each polarization direction. This causes a difference in the reflection characteristics of each polarization. In contrast, the proposed LC IRS controls the reflection characteristics by changing the electric thickness of the reflecting element. Owing to its configuration, the proposed LC IRS can control reflection characteristics while maintaining a symmetrical configuration in each orthogonal polarization direction. In addition, since the TFT on the reflecting element controls the bias voltage in 256 steps, the reflection phase of the proposed IRS can control 256 steps of the reflection phase. This enables continuous control of the reflection direction.

The main contributions of this paper are as follows:

1) Proposal of the design of the dual-polarized LC IRS

It has an asymmetric configuration to control the reflection characteristics of each polarization equally.

1) Derivation of an equivalent circuit model of the LC IRS for design method with the equivalent circuit
2) Verification of the LC IRS through an EM simulator

It can control a reflection phase of more than 260 degrees for each polarized signal.

1) Development of the proposed LC IRS
2) Verification of the LC IRS through measurement in an anechoic chamber

The proposed IRS controls the reflection direction of each polarized signal over a wide range of ± 60 degrees with a high isolation of approximately 20 dB.

1) Derivation of the channel capacity of the proposed IRS

The proposed IRS can control the reflection direction maintaining channel capacity high.

On the other hand, since the reflection amplitude of the proposed IRS drops 7 dB depending on the bias voltage. This causes the reflection loss. In addition, the response time of the liquid crystal is larger than semiconductor switches. These hardware limitations are considered as future works.

REFERENCES

[1] *Studies on Frequency-Related Matters for International Mobile Telecommunications Identification Including Possible Additional Applications to the Mobile Service on Primary Basis Portion(s) of the Frequency Range Between 24.25 and 86 GHz for the Future Development of International Telecommunication for 2020 and Beyond*, 2015.

[2] S. Rangan, T. S. Rappaport, and E. Erkip, "Millimeter-wave cellular wireless networks: Potentials and challenges," *Proc. IEEE*, vol. 102, no. 3, pp. 366–385, Mar. 2014.

[3] C. K. Anjinappa, F. Erden, and I. Guvenç, "Base station and passive reflectors placement for urban mmWave networks," *IEEE Trans. Veh. Technol.*, vol. 70, no. 4, pp. 3525–3539, Apr. 2021.

[4] A. Gómez-Andrades, R. Barco, and I. Serrano, "A method of assessment of LTE coverage holes," *EURASIP J. Wireless Commun. Netw.*, vol. 2016, no. 1, pp. 1–12, Dec. 2016.

[5] Q. Wu and R. Zhang, "Towards smart and reconfigurable environment: Intelligent reflecting surface aided wireless network," *IEEE Commun. Mag.*, vol. 58, no. 1, pp. 106–112, Jan. 2020.

[6] M. Di Renzo, A. Zappone, M. Debbah, M. Alouini, C. Yuen, J. de Rosny, and S. Tretyakov, "Smart radio environments empowered by reconfigurable intelligent surfaces: How it works, state of research, and the road ahead," *IEEE J. Sel. Areas Commun.*, vol. 38, no. 11, pp. 2450–2525, Nov. 2020.

[7] R. Liu, J. Dou, P. Li, J. Wu, and Y. Cui, "Simulation and field trial results of reconfigurable intelligent surfaces in 5G networks," *IEEE Access*, vol. 10, pp. 122786–122795, 2022.

[8] A. Araghi, M. Khalily, M. Safaei, A. Bagheri, V. Singh, F. Wang, and R. Tafazolli, "Reconfigurable intelligent surface (RIS) in the sub-6 GHz band: Design, implementation, and real-world demonstration," *IEEE Access*, vol. 10, pp. 2646–2655, 2022.

[9] R. Liu, Q. Wu, M. Di Renzo, and Y. Yuan, "A path to smart radio environments: An industrial viewpoint on reconfigurable intelligent surfaces," *IEEE Wireless Commun.*, vol. 29, no. 1, pp. 202–208, Feb. 2022.

[10] M. Jian, R. Liu, and Y. Chen, "Standardization for reconfigurable intelligent surfaces: Progresses, challenges and the road ahead," in *Proc. IEEE/CIC Int. Conf. Commun. China (ICCC Workshops)*, Xiamen, China, Jul. 2021, pp. 337–342.

[11] E. G. Larsson, O. Edfors, F. Tufvesson, and T. L. Marzetta, "Massive MO for next generation wireless systems," *IEEE Commun. Mag.*, vol. 52, no. 2, pp. 186–195, Feb. 2014.

[12] Y. Li, Q. Cao, and Y. Wang, "A wideband multifunctional multilayer switchable linear polarization metasurface," *IEEE Antennas Wireless Propag. Lett.*, vol. 17, no. 7, pp. 1314–1318, Jul. 2018.

[13] W. Tang, M. Z. Chen, X. Chen, J. Y. Dai, Y. Han, M. Di Renzo, Y. Zeng, S. Jin, Q. Cheng, and T. J. Cui, "Wireless communications with reconfigurable intelligent surface: Path loss modeling and experimental measurement," *IEEE Trans. Wireless Commun.*, vol. 20, no. 1, pp. 421–439, Jan. 2021.

[14] A. Xia, Z. Wang, S. Geng, X. Zhao, R. Zhang, Y. Liu, and Y. Geng, "28 GHz MIMO channel capacity analysis for 5G wireless communication systems," in *Proc. 12th Int. Symp. Antennas, Propag. EM Theory (ISAPE)*, Hangzhou, China, Dec. 2018, pp. 1–4.

[15] Y. Han, X. Li, W. Tang, S. Jin, Q. Cheng, and T. J. Cui, "Dual-polarized RIS-assisted mobile communications," *IEEE Trans. Wireless Commun.*, vol. 21, no. 1, pp. 591–606, Jan. 2022.

[16] S. Gong, X. Lu, D. T. Hoang, D. Niyato, L. Shu, D. I. Kim, and Y. Liang, "Toward smart wireless communications via intelligent reflecting surfaces: A contemporary survey," *IEEE Commun. Surveys Tuts.*, vol. 22, no. 4, pp. 2283–2314, 4th Quart., 2020.

[17] L. Dai, B. Wang, M. Wang, X. Yang, J. Tan, S. Bi, S. Xu, F. Yang, Z. Chen, M. D. Renzo, C. Chae, and L. Hanzo, "Reconfigurable intelligent surface-based wireless communications: Antenna design, prototyping, and experimental results," *IEEE Access*, vol. 8, pp. 45913–45923, 2020.

[18] X. Chen, J. C. Ke, W. Tang, M. Z. Chen, J. Y. Dai, E. Basar, S. Jin, Q. Cheng, and T. J. Cui, "Design and implementation of MIMO transmission based on dual-polarized reconfigurable intelligent surface," *IEEE Wireless Commun. Lett.*, vol. 10, no. 10, pp. 2155–2159, Oct. 2021.

[19] X. Li, H. Sato, Y. Shibata, T. Ishinabe, H. Fujikake, and Q. Chen, "Development of beam steerable reflectarray with liquid crystal for both E-plane and H-plane," *IEEE Access*, vol. 10, pp. 26177–26185, 2022.

[20] H. Matsuno, T. Ohto, Y. Amano, M. Okita, D. Suzuki, K. Matsunaga, and S. Oka, "Development of a direction-variable liquid crystal meta-surface reflector," in *Proc. IEEE Int. Conf. Commun.*, May 2022, pp. 4854–4859.

[21] M. Okita, D. Suzuki, K. Matsunaga, S. Oka, H. Matsuno, and T. Ohto, "Development of reconfigurable liquid crystal metasurface reflector based on TFT-LCD technology," in *Proc. SPIE*, vol. 12442, Mar. 2023, Art. no. 1244205.

[22] *Dassault Systems, CST Studio Suite*.

[23] T. Bai and R. W. Heath, "Coverage and rate analysis for millimeter-wave cellular networks," *IEEE Trans. Wireless Commun.*, vol. 14, no. 2, pp. 1100–1114, Feb. 2015.

[24] Y. Okano and K. Cho, "Dependency of MIMO channel capacity on XPR around mobile terminals for multi-band multi-antenna," in *Proc. 2nd Eur. Conf. Antennas Propag. (EuCAP)*, 2007, pp. 1–6.

[25] *Guidelines for Evaluation of Radio Interface Technologies for IMT-2020*, document 2412-0, Oct. 2017.

[26] C. Fritzsch, B. Snow, J. Sargent, D. Klass, S. Kaur, and O. Parri, "Liquid crystals beyond displays: Smart antennas and digital optics," in *Proc. SID*, 2019, pp. 1098–1101.

[27] R. Reese, E. Polat, H. Tesmer, J. Strobl, C. Schuster, M. Nickel, A. B. Granja, R. Jakoby, and H. Maune, "Liquid crystal based dielectric waveguide phase shifters for phased arrays at W-band," *IEEE Access*, vol. 7, pp. 127032–127041, 2019.

[28] O. Karabey, A. Gaebler, and R. Jakoby, "A 2-D electronically steered phased-array antenna with 2×2 elements in LC display technology," *IEEE Trans. Microw. Theory Techn.*, vol. 60, no. 5, May 2012, pp. 1297–1306.

[29] R. Kuse, T. Hori, M. Fujimoto, T. Seki, K. Sato, and I. Oshima, "Equivalent circuit analysis for alternated double layer patch type FSS with dielectric substrate," in *Proc. IEEE Antennas Propag. Soc. Int. Symp. (APSURSI)*, Jul. 2014, pp. 2082–2083.

HIROMI MATSUNO received the B.E., M.E., and Ph.D. degrees from Yokohama National University, Japan, in 2005, 2007, and 2010, respectively. After joining the KDDI Research and Development Laboratories (currently KDDI Research Inc.), in 2010, he engaged in research and development in the field of base station antenna for 4G and 5G mobile communication systems. In 2015, he joined the Advanced Telecommunication Research Institute International (ATR), where he was engaged in dynamic spectrum sharing and localization. In 2018, he joined KDDI Research Inc. He is currently involved in research and development in the field of reconfigurable intelligent surface and antennas for beyond 5G/6G mobile communication systems. He received the Meritorious Award on Radio from the Association of Radio Industries and Businesses (ARIB), in 2021.

TAKUYA OHTO (Member, IEEE) received the B.E. degree in electrical and electronic engineering from Kyoto University, in 2015, and the M.E. degree from the Graduate School of Informatics, Kyoto University, in 2017. He was an Employee with KDDI Corporation. In 2020, he joined KDDI Research Laboratories Inc. His current research interests include millimeter-wave wireless communications and reconfigurable intelligent surfaces. He is a member of the IEICE.

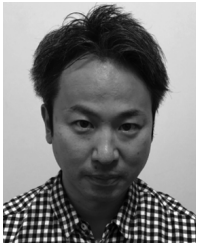

TAKAHIRO HAYASHI received the B.E. and M.E. degrees in information and communication engineering from Yokohama National University, Japan, in 2002 and 2004, respectively. In 2004, he joined KDDI Corporation, where he was engaged in telecommunication network planning and optimization. Since 2010, he has been engaged in the research and development of mobile communication systems with KDDI Research Inc. He is currently involved in the development of new frequency bands and radio propagation prediction by using machine learning. He received the Young Researcher's Award from IEICE, in 2011.

YOSHIAKI AMANO received the B.E. and M.E. degrees in electrical and electronic engineering from Nagoya University, Aichi, Japan, in 1995 and 1999, respectively. He joined KDD Corporation (currently KDDI Corporation), in 1999, where he was involved in research and development on CDMA cellular systems, smart antenna, and wireless performance evaluation and improvement of mobile terminals. He also engaged with the Energy Business Planning Division, KDDI Corporation, to launch the electric power retail business, from 2015 to 2018. Since 2018, he has been launching research and development on dynamic spectrum sharing systems and intelligent reflecting surface with KDDI Research Inc., before he has led research on wireless communication systems for beyond 5G/6G. He received the Young Researcher's Award from IEICE and the Meritorious Award on Radio from the Association of Radio Industries and Businesses (ARIB), in 2005 and 2011, respectively.

MITSUTAKA OKITA was born in Osaka, Japan, in 1970. He received the B.S. and M.S. degrees in electronic engineering from Tohoku University, Sendai, Japan, in 1993 and 1995, respectively. From 1995 to 2011, he was a LCD Design Development Engineer with Panasonic and Toshiba Mobile Display. Since 2012, he has been with Japan Display Inc. His research interests include the development of advanced liquid crystal displays, such as wide viewing angle LCDs and fast response LCDs.

DAIICHI SUZUKI was born in Shizuoka, Japan, in 1975. He received the B.S. and M.S. degrees in electrical engineering from Waseda University, Tokyo, Japan. From 1999 to 2011, he was a Researcher with the Panasonic Research Laboratory and Toshiba Mobile Display's Research and Development Center. Since 2012, he has been with Japan Display Inc., and currently the Engineering Manager. His research interest includes the development of LCDs. He has been a member of SID Committee for LC Technologies, since 2020.

KAZUKI MATSUNAGA was born in Chiba, Japan, in 1991. He received the B.S. and M.S. degrees in engineering from Chiba University, in 2014 and 2016, respectively. Since 2016, he has been a Researcher with Japan Display Inc. His research interests include the development of flexible displays and optical sensors.

SHINICHIRO OKA was born in Sendai, Miyagi, Japan, in 1977. He received the B.S. and M.S. degrees in electrical engineering and the Ph.D. degree in material engineering from the Nagaoka University of Technology, in 1998, 2001, and 2004, respectively. Since 2004, he has been a Researcher with the Hitachi Research Laboratory. He was a Distinguished Researcher with the Hitachi Research Laboratory, in 2013. Since 2014, he has been with Japan Display Inc. He is currently with Japan Display Inc., as the Senior Manager. His research interests include the development of liquid crystal displays, 3D displays, and flexible displays.